Interface crossing behavior of prolate microswimmers: Thermo and hydrodynamics

Rishish Mishra, Harish Pothukuchi, Harinadha Gidituri, Juho S. Lintuvuori

Interface crossing behavior of prolate microswimmers: thermo and hydrodynamics

Rishish Mishra and Harish Pothukuchi
Department of Mechanical Engineering, Indian Institute of Technology Jammu 181221, India.

Harinadha Gidituri*
Department of Chemical Engineering, Birla Institute of Technology Pilani, Hyderabad Campus 500078, India

Juho Lintuvuori†
Univ. Bordeaux, CNRS, LOMA, UMR 5798, F-33400 Talence, France

We study the dynamics of prolate microswimmers traversing clean liquid-liquid interfaces. Using large-scale lattice Boltzmann simulations, we observe that the swimmers can be either trapped or cross the interface, depending on their initial angle, swimming speed, and the interfacial tension between the two fluids. The simulation results are rationalized by considering a competition between interfacial (thermodynamic) and self-propulsion (hydrodynamic) forces. The swimmers get trapped at the interface due to a thermodynamic trapping force, similar to trapping of passive colloidal particles at interfaces, when the forces from the interfacial tension dominate over the swimming forces. The trapping behavior can be captured by calculating a critical capillary number, which involves balancing the interfacial and self-propulsion forces. This prediction agrees remarkably well with the numerical simulations. Finally, our results demonstrate that the torque resulting in a reorientation of the swimmers parallel to the interface has both hydro and thermodynamic components.

I. INTRODUCTION

The motility of microorganisms in an aqueous environment is important for their evolution. The locomotion helps them in seeking nutrient-rich hot spots, for reproduction and to escape from protist predators. In particular, their motion strongly depends on the feedback mechanism from the surrounding environment [1]. Such feedback can result from any source, for example, another particle (passive or active) in the vicinity or a surface such as a wall [2] or fluid-fluid interface [3, 4]. It is well known from the previous experimental [5–7] and numerical studies [8–10] that hydrodynamics dictates the movement of microorganisms such as bacteria when swimming close to a no-slip wall or to fluid-fluid interfaces. Specifically, during the interaction with the fluid-fluid interface, in addition to hydrodynamics, thermodynamics also modifies the dynamic behavior of micro-particles (passive and active) [11]. Sometimes these microswimmers gets adsorbed from the bulk onto the interface and straddle upon it [12–14]. For neutrally wetting colloidal particles, thermodynamics drives such an adsorption process by reducing the available interfacial area, which in turn reduces the interfacial energy [15–18].

The interaction between microswimmer and interface has recently attracted significant interest due to its applications, including biofilm formation [19], biomedical applications [20], and environmental remediation [21–23]. Motivated by this, several researchers have explored the interactions of microswimmers at and near the interface, encompassing experimental [5–7, 13], theoretical [3, 24, 25], and numerical approaches[9, 10, 26–28]. For instance, Shaik and Ardekani [3] studied the hydrodynamic behavior of a microswimmer near a weakly deformable interface. Using a time-reversible squirmer, they reported swimmer either moves towards or away from the interface, depending upon its initial velocity and orientation. Similarly, Desai *et al.* [29] investigated the hydrodynamics of microswimmers modeled as a force dipole near a drop and found that the swimmers orbit around or scatter away, subject to the drop radius (critical trapping radius) and basin of attraction. They concluded that the influence of hydrodynamic attraction does not extend beyond three body length of the swimmer. Further, Feng *et al.* numerically investigated the dynamics of a spherical microswimmer near a liquid-liquid interface with [10] and without [9] the viscosity contrast. They observed different swimming states such as, bouncing, penetrating, hovering, and sliding over the interface. These states are presented as a function of incident angle and microswimmer type. Given that microswimmers can exhibit a variety of shapes, Nambiar and Wettlaufer [4] studied the hydrodynamics of a slender-shaped microswimmer near

* g.harinadha@hyderabad.bits-pilani.ac.in
† juho.lintuvuori@u-bordeaux.fr

a deformable fluid-fluid interface. Their results reveal the mutual interaction (attraction and repulsion) between the swimmer and the interface (deformation), governed by the swimmer's configuration, position, and type (pusher or puller). Later, they also analyzed the role of different types of stochasticities (random tumble and active Brownian) on the reorientation behavior of the microswimmer [30]. Their findings revealed that both rotational and positional shifts occurred, either toward or away from the interface.

While these studies have clearly analyzed the hydrodynamics interaction between the microswimmer and the fluid-fluid interface, however the role of the interfacial trapping forces, arising from the wetting is often neglected. A recent experimental study, Cheon *et al.* [6] examined the interaction between a rod-shaped bacterium *Bacillus subtilis* with a liquid-liquid interface consisting of a coexisting isotropic-nematic phase. The results demonstrated that bacteria can either be trapped or cross the interface depending on their velocity and initial projection angle. The trapping results were rationalized considering an interfacial force and torque that arise from an interfacial deformation created by the bacteria pushing on the interface between the isotropic and nematic states [6]. Further, the competition between the interfacial and active forces has been observed to lead to a repartition of *Bacillus subtilis* in binary fluids consisting of dextran (DEX) and polyethylene glycol (PEG) interfaces [7].

Motivated by these experiments, we study the trapping dynamics of a rod-like microswimmer at clean liquid-liquid interfaces. We demonstrate that the trapping dynamics of the swimmers is dominated by a wetting mediated trapping energy, akin to trapping of passive colloidal particles at liquid-liquid interfaces [31]. It can be captured by considering a capillary number based on the ratio between a swimming force and and a force arising from the interfacial tension σ_0 between the two fluids: $\mathrm{Ca} = u_0\eta/\sigma_0$, where u_0 is the swimming speed of the bacteria and η is the fluid viscosity. When the thermodynamic forces arising from the interfacial tension dominate, the swimmer is trapped. Further, we show that the rotational dynamics of the swimmers, arise from combined thermo and hydrodynamic torques.

A. Simulation Model and details

To study the microswimmer dynamics we use the lattice Boltzmann method (LBM)[32, 33]. To take care of the swimmer geometry, the prolate swimmer is modeled as a 3-dimensional ellipsoid described by an equation $\frac{x'^2}{a^2} + \frac{y'^2}{b^2} + \frac{z'^2}{c^2} = 1$ where $a > b = c$, with a and b being the semi-major and semi-minor axes, respectively. The aspect ratio of the prolate is defined as $AR = \frac{a}{b}$. In the present work, we fix the value of AR at 3 with $b = 4$.

Hydrodynamics of the prolate microswimmer under Stokes flow is captured using the spheroidal squirmer model [34]. In this scheme, a microswimmer is considered as a solid prolate particle with a prescribed slip velocity on the boundary, defined as following

$$v_s = -B_1(\mathbf{s}.\hat{e})\mathbf{s} - B_2\zeta(\mathbf{s}.\hat{e})\mathbf{s} \tag{1}$$

where $\hat{e}$ is along the major axis. The surface tangent vector $\mathbf{s}$ is given as,

$$\mathbf{s} = -\frac{\sqrt{a^2 - z'^2}}{\sqrt{a^2 - \epsilon^2 z'^2}}\hat{e} + \frac{\sqrt{1-\epsilon^2}}{\sqrt{a^2 - \epsilon^2 z'^2}} z' \hat{e}_\perp$$

when the major axis of prolate particle $\hat{e}$ is oriented along z' axis[35]. The spheroidal coordinate system term $\zeta = [\sqrt{x'^2 + y'^2 + (z' + a\epsilon)^2} - \sqrt{x'^2 + y'^2 + (z' - a\epsilon)^2}]/2a\epsilon$.

The amplitudes of the slip velocity, B_1 and B_2 are the first two squirming modes, representing the source and force dipoles, respectively. The ratio of these two squirming modes, $\dfrac{B_2}{B_1}$, is called the squirmer coefficient, denoted by β. This coefficient can be varied to model different types of microswimmers, such as pusher ($\beta < 0$), puller ($\beta > 0$), and neutral ($\beta = 0$). However, in the current study, we kept the β value at -1. Such a choice is motivated from the experiments [6] on Bacteria (*Bacillus subtilis*), which is of a pusher type. The swimming speed u_0 for a prolate microswimmer

$$u_0 = B_1\epsilon^{-1}(\epsilon^{-1} - (\epsilon^{-2} - 1)\coth^{-1}(\epsilon^{-1})),$$

where $\epsilon = \sqrt{1 - \frac{1}{AR^2}}$[36].

Next, a cubical simulation box with dimensions $160 \times 160 \times 160$ is considered, where the interface is positioned at the center of the box. The box has periodic boundaries in two directions, while solid wall boundaries are applied along the plane parallel to the interface. The projection angle ϕ_0 is defined as the angle between the interface and the microswimmer orientation ($\hat{e}$) along the major-axis (Fig. 1).

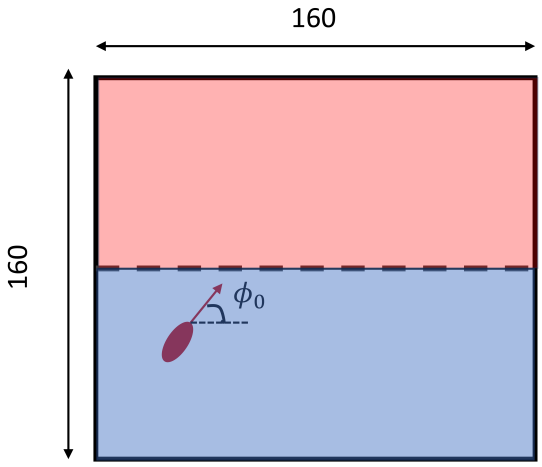

FIG. 1. A prolate microswimmer approaching towards the interface separating two fluids with self-propulsion velocity u_0 and initial projection angle ϕ_0.

The existence of an interface is due to the presence of two immiscible fluids. To model the interface of a binary fluid mixture, the Ginzburg-Landau type free energy functional is used [33] and is given as below.

$$F = \int dV \left(-\frac{A}{2}\psi^2 + \frac{B}{4}\psi^4 + \frac{\kappa}{2}|\nabla\psi|^2 \right) \tag{2}$$

Here ψ is the phase field variable. The temporal evolution of ψ is governed by the Cahn-Hilliard equation,

$$\partial_t\psi + \mathbf{U}\cdot\nabla\psi = M\nabla^2\mu \tag{3}$$

where $\mathbf{U}$ is the fluid velocity, M is the mobility, and μ is the chemical potential derived from the free energy functional in Eq. (2) by $\mu = \frac{\delta F}{\delta\psi} = A\psi + B\psi^3 - \kappa|\nabla^2\psi|$. The fluid velocity is obtained by solving the Navier-Stokes equation.

$$\rho(\partial_t\mathbf{U} + \mathbf{U}\cdot\nabla\mathbf{U}) = -\nabla P + \eta\nabla^2\mathbf{U} - \psi\nabla\mu \tag{4}$$

where, the gradient of the hydrodynamic pressure P is supplemented by a thermodynamic force $\psi\nabla\mu$. The simulations are carried out using a hybrid method, where ψ is solved by finite difference and $\mathbf{U}$ arises from lattice Boltzmann. We used open source lattice Boltzmann code Ludwig (version 0.21.0) to carry out the simulations [37, 38].

For all the simulations reported in this work, the viscosities of both phases ($\psi = +1$ and $\psi = -1$) are maintained at a constant value $\eta = 0.625$ and their densities are set to unity $\rho = 1$. The simulations are carried under low Reynolds number assumption, $\mathrm{Re} = \frac{\rho u_0 a}{\eta} \sim 10^{-2}$. The capillary number $\mathrm{Ca} = \frac{\eta u_0}{\sigma_0}$ where $\sigma_0 = \sqrt{\frac{8\kappa|A|^3}{9B^2}}$ denotes an interfacial tension. Ca was varied by two different ways: modifying the interfacial tension while keeping the self-propulsion velocity constant, and in the other case varying the swimming velocity for a constant interfacial tension. In the first case, the parameters of the binary fluid interface, including the bulk free energy coefficients, are varied within the range $A = -B = -4.9 \times 10^{-3}$ to -0.019, and the interface penalty κ is varied from 4.8×10^{-3} to 0.0189. This results to interfacial tensions $\sigma_0 \approx 4.6 \times 10^{-3}$ to 0.018, while keeping the velocity $u_0 = 8.9 \times 10^{-4}$ constant. In the second case, the interfacial tension is fixed at $\sigma_0 \approx 0.012$, with $A = -B = -0.0133$ & $\kappa = 0.013$ while the propulsion velocity u_0 is incremented between 5.7×10^{-4} and 0.0023. For all the simulations the mobility parameter in the Cahn-Hilliard Eq. 3 $M = 0.5$ and the interfacial width $\chi_0 = \sqrt{\frac{2\kappa}{|A|}} \approx 1.4$ were kept constant. The latter gives a Cahn number $\mathrm{Cn} = \chi_0/a \approx 0.1$, where a is the half-length of the swimmer. This compares favorably to reported experimental numbers of Bacillus subtilis interacting with PEG-DEX interfaces [7] $\chi_0 \sim 1$ μm and bacterial length ~ 10 μm, giving $\mathrm{Cn} \approx 0.2$.

Quantity	Value in LU	Conversion Factor	Value in SI Units
Swimmer half-length (a)	12	$L^* = 0.5$ μm	6 μm
Swimmer half-width (b)	4	$L^* = 0.5$ μm	2 μm
Interfacial width (χ_0)	1.4	$L^* = 0.5$ μm	0.7 μm
Velocity (u_0)	5.7×10^{-4} to 2.3×10^{-3}	$u^* = 1$ m/s	5.7×10^{-4} to 2.3×10^{-3} m/s
Dynamic Viscosity (η)	0.625	$\eta^* = 5 \times 10^{-4}$ Pa $\cdot$ s	3.12×10^{-4} Pa $\cdot$ s
Interfacial Tension (σ_0)	4.6×10^{-3} to 1.8×10^{-2}	$\sigma_0^* = 5 \times 10^{-4}$ N/m	2.3 to 9 μN/m

TABLE I. Conversion of lattice units (LU) to corresponding physical quantities in SI units.

Assuming a typical bacterial length $\approx 12\mu$m, we can map a simulation length unit to SI units using 12 μm/24 LU = 0.5μm. Using the density and viscosity of water, and setting Re $\approx 10^{-2}$ gives conversion factors 1m/s, 5×10^{-4}Pa $\cdot$ s and 5×10^{-4}N/m for velocity, dynamic viscosity and interfacial tension, respectively. The key simulation parameters with their mapping to SI units are given in table I.

II. RESULTS AND DISCUSSION

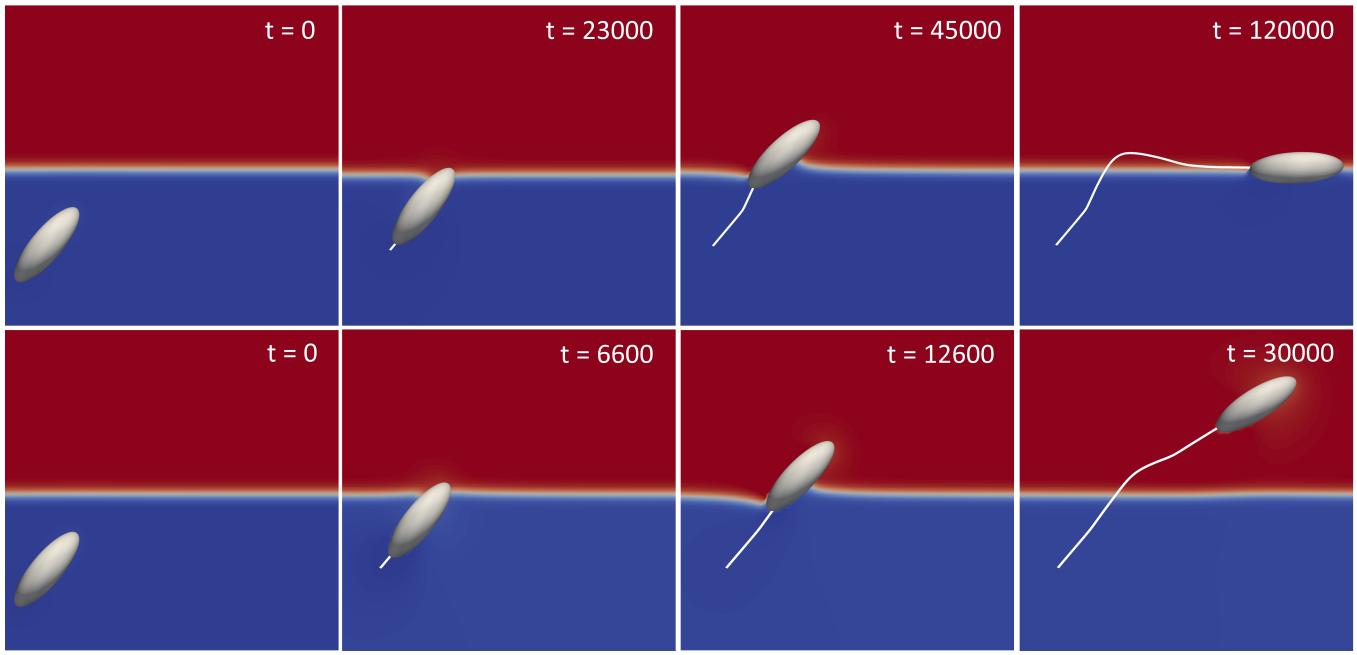

FIG. 2. Snapshots showing a neutrally wetting microswimmer either being trapped or crossing a clean liquid-liquid interface, for Ca ≈ 0.03 (top row) and Ca ≈ 0.12 (bottom row) respectively. The initial projection angle is $\phi_0 = 50^\circ$ and the interfacial tension $\sigma_0 \approx 6$ μN/m.

We study the dynamics of a rod-like prolate-shaped swimming particle approaching a fluid-fluid interface at different Ca $= \eta u_0/\sigma_0$ and initial projection angles ϕ_0. The particle was initialized at vertical distance $5b$ below the interface and its initial aligned angle ϕ_0 was varied (Fig. 1). We consider swimmers that have equal affinity to both fluids, corresponding to a contact angle $\theta \approx 90^\circ$ at the interface, which is similar to the experiments [6]. When a swimmer reaches an interface, it penetrates the second fluid in and the contact angle between the two fluids and the particle surface adopts $\approx 90^\circ$ (see intermediate times in Fig. 2). When the interfacial forces dominate, the particle is trapped, and eventually aligns parallel along the interface (see Ca ≈ 0.03 case (top row) in Fig. 2). When the self-propulsion speed is increased, the swimmer can swim across the interface (see Ca ≈ 0.12 case (bottom row) in Fig. 2).

To study the dynamics, the particle trajectories were recorded across multiple capillary numbers and initial alignment angles ϕ_0 (Fig. 3). When the swimmers are initially close to perpendicular to the interface, large ϕ_0, we observe a smooth crossing of the interface, while for small shallow angles the swimmers get trapped at the interface (Fig. 3i).

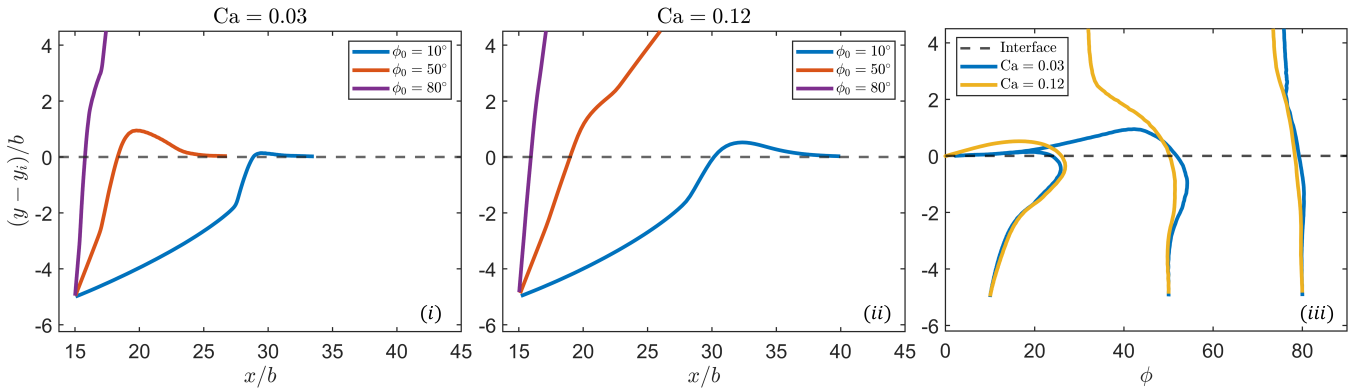

FIG. 3. Trajectories in $x - y$ space of a prolate swimmer for (i) Ca ≈ 0.03 and (ii) Ca ≈ 0.12 as well as (iii) in $\phi - y$ space, for initial alignment angles $\phi_0 \approx 10°$, $50°$ and $80°$, where y_i is the interface position. The data corresponds to interfacial tension $\sigma_0 \approx 6$ μN/m and aspect ratio $AR = 3$.

The critical angle ϕ_0 when this happens, depends on the capillary number (Fig. 3ii). When the Ca is reduced, the interfacial (trapping) forces dominate over the swimming forces and the swimmers are observed to be trapped at larger alignment angles (Fig. 3i). Additionally, reorientation of the swimmer occurs along its trajectory (Fig. 3iii). Typically, the swimmer reorients towards the parallel of the interface, in agreement with previous simulations [9]. Interestingly, at shallow angles we observe initial reorientation towards the interface normal when the particle is well below the interface, followed by realignment parallel to the interface after the particle has been trapped (see *e.g.,* $\phi_0 \approx 10°$ curves in Fig. 3iii). The initial reorientation likely arises from the far-field hydrodynamics.

To understand the trapping in more detail, we mapped a phase diagram as a function of the capillary number Ca and initial alignment angle ϕ_0 (Fig. 4). As it is mentioned in the previous section (Sec. I A) we considered two set of simulations: one where the capillary number Ca $= u_0\eta/\sigma_0$ is calculated by varying the interfacial tension σ_0 for a constant velocity u_0 (blue symbols in Fig. 4) and other by varying u_0 while keeping σ_0 constant (red symbols in Fig. 4).

A. Wetting induced thermodynamic trapping

We hypothesize that the observed trapping/crossing dynamics arise from the balance between interfacial trapping and active swimming forces. Considering a passive spherical particle with a radius R at height $h < R$ below a liquid-liquid interface eliminates a planar area $\pi\left(R^2 - h^2\right) = \pi R^2\left(1 - \cos\theta\right)^2$ from the interface, where θ is related to the contact angle between the two fluids and the particle surface. Considering an interface with an interfacial tension σ_0, removing the particle into the lower fluid has an energetic cost $E = \pi R^2\sigma_0\left(1 - \cos\theta\right)^2$ [31]. For neutrally wetting particles, $\theta \approx 90°$, as in our simulations, this gives a trapping energy $E = \pi R^2\sigma_0$.

We assume that this is the dominant trapping mechanism in our simulations. For a prolate swimmer, the area removed from the interface takes the shape of an ellipse and depends both on the aspect ratio a/b as well as the alignment angle, ϕ [39]

$$A_{\rm rm}(\phi) = \frac{\pi a b^2}{\sqrt{b^2\cos^2\phi + a^2\sin^2\phi}}. \tag{5}$$

This gives an angle-dependent trapping energy

$$E^p_{\rm th}(\phi) = A_{\rm rm}(\phi)\sigma_0, \tag{6}$$

where the thermodynamic trapping increases with decreasing ϕ and reaches the maximum when the rod-like particle is parallel to the interface $\phi \approx 0$.

In order the swimmers to escape a thin interface, they need to swim a distance $L_{\rm eff} = \sqrt{a^2\sin^2\phi + b^2\cos^2\phi}$, corresponding to a half-length of an ellipsoid perpendicular to the interface, to overcome the energy barrier with a height $E^p_{\rm th}$. We can now estimate the magnitude of the trapping force as $F_{\rm int} \approx E^P_{\rm th}/L_{\rm eff}$. The self-propulsion force of the swimmers perpendicular to the interface, can be estimated using Stokes' law: $F_{\rm swim} \approx \mu_{\rm trans}u_0\sin\phi$, where

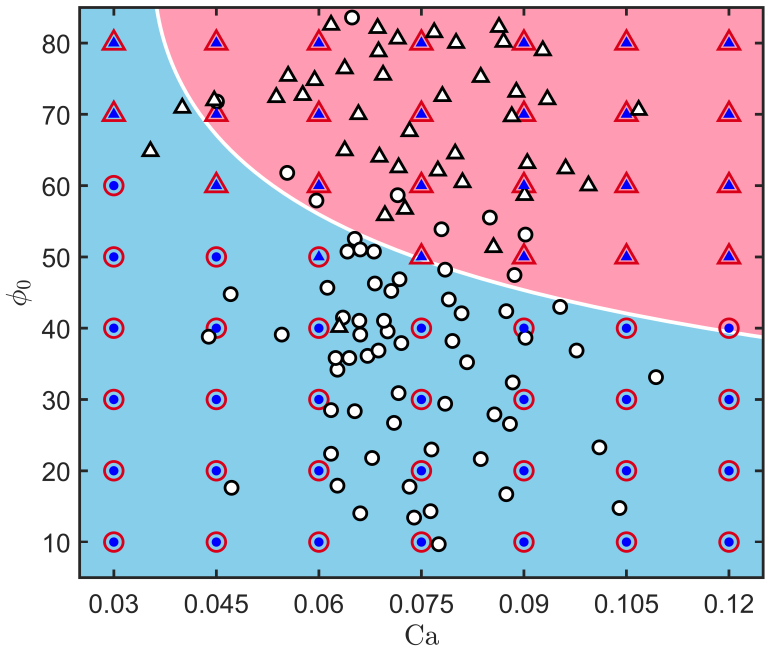

FIG. 4. A state diagram of a prolate microswimmer showing crossing (triangles) and trapped (circles) states as a function of the capillary number $\mathrm{Ca} = u_0\eta/\sigma_0$ and initial alignment angle ϕ_0. The red (blue) symbols correspond to simulations where the swimming speed u_0 (interfacial tension σ_0) was varied. The white symbols represent the experiments of Bacillus Subtilis crossing an isotropic-nematic interface [6]. The solid white line represents a critical capillary number, calculated from a balance between swimming (self-propulsion) and interfacial (trapping) forces (Eq. 7; see text for details).

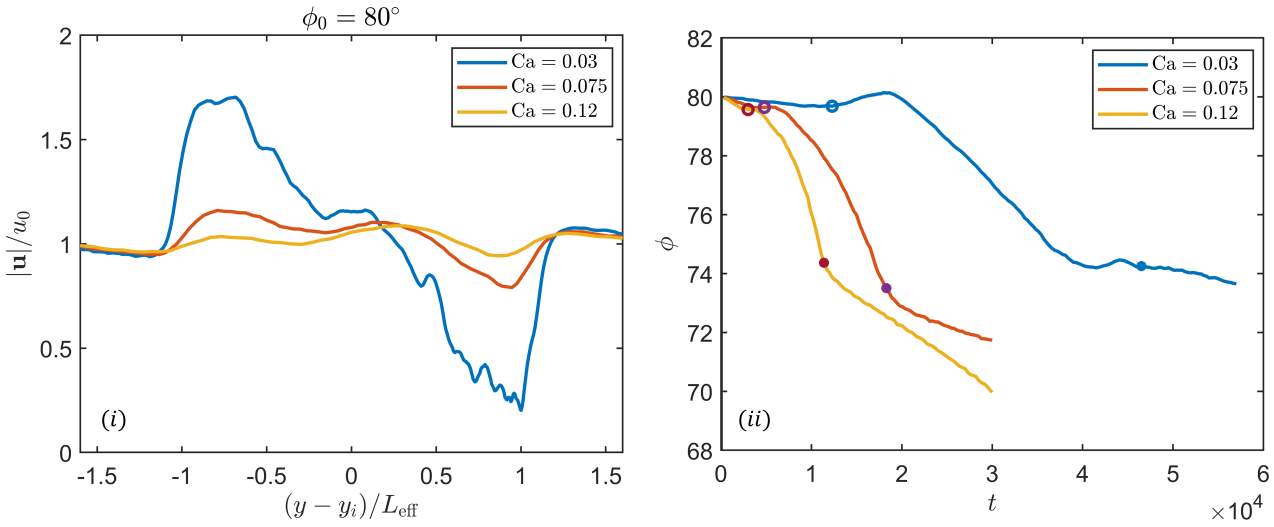

FIG. 5. (i) The normalized velocity shows the fluctuations when the prolate swimmer crosses the interface located at $y \approx y_i$. (ii) Temporal evolution of the orientation ϕ of the microswimmer during the interaction with the interface, where $\sigma_0 \approx 6$ μN/m. The open and closed circles indicate the particle-interface interaction onset and offset points, respectively. The onset and offset points are at $y{\approx}y_i \mp L_{\mathrm{eff}}$, below and above the interface.

$\mu_{\mathrm{trans}} = \frac{4\pi\eta a}{\ln\frac{2a}{b} - 0.5}$ denotes the translational drag coefficient of a prolate particle moving along its major axis [40], and $u_0 \sin\phi$ is the speed perpendicular to the interface. When the swimming force is larger than the trapping force, the swimmer can escape the interface. By equating these two competing forces, we can estimate a critical capillary

number Ca^*

$$(4\mathrm{Ca}^*)^{-1} = \frac{\sin\phi(a^2\sin^2\phi + b^2\cos^2\phi)}{b^2(\ln(\frac{2a}{b}) - 0.5)}. \tag{7}$$

which predicts the boundary between the crossing and trapped states (solid white line in Fig. 4), and agrees very well with the simulation data (blue and red symbols in Fig. 4).

Interestingly, our simulations and the equation 7 agree reasonably well also with the experimental observations of *Bacillus subtilis* crossing an isotropic-nematic interface [6] (white symbols in Fig. 4). To compare to the bacterial experiments, we converted the data given in Fig. 2 in [6] using the supplementary figure S8 with the reported values for swimming speed 15–35 $\mu\mathrm{m\,s}^{-1}$, viscosity $\eta \approx 30\mathrm{mPas}$ and interfacial tension $\sigma_0 \approx 10\mu\mathrm{Nm}^{-1}$ [6]. Even if the agreement is reasonably good, we should note that we consider an interface between two Newtonian fluids, and the dynamics is dominated by a wetting-mediated interfacial trapping force, similar to trapping of passive particles at liquid-liquid interfaces. On the other hand, while in the experiments the swimmers have a contact angle $\approx 90^\circ$, the interface is between an isotropic fluid and a non-Newtonian (nematic) phase. The experimental observations were explained by a mechanical argument based on a repulsive force and a corresponding torque arising from a deformation created by the tip of the bacteria pushing onto the interface [6].

B. Swimmer dynamics

The dynamics of the swimmer is strongly influenced by the presence of a liquid-liquid interface. During the early stages of the trajectory, a swimmer speeds up at the onset of particle-interface interaction and then slows down until complete separation from the interface (Fig. 5i). This is consistent with a thermodynamic potential corresponding to trapping of neutrally wetting particles at liquid-liquid interfaces [31]. When the Capillary number Ca increases, the overall change in swimming velocity during interface crossing decreases (Fig. 5i). This likely arises from hydrodynamic effect between the swimmer and the interface.

The changes in the translational motion are accompanied by rotational motion (Fig 5ii). The swimmers are observed to reorient towards the interface. This is in agreement with previous studies [8, 9], where spherical pusher-type microswimmers, have been observed to reorient parallel to an interface due to a hydrodynamic torque. However, in the case of a prolate-shaped swimmer, rotational motion can have an additional thermodynamic component. Additionally, it is interesting to note that the exit angle of the swimmer traversing the interface remains approximately same, whereas the rate of orientation increases with increasing capillary number Ca (Fig. 5ii). This can be understood by considering that the capillary number is modified by increasing the swimming speed $u_0 \sim B_1$, while the ratio between the force and source dipoles $\beta = B_2/B_1 \approx -1$ is kept constant. The hydrodynamic torque of a swimmer at an interface, is predicted to scale linearly with the force dipole strength $\sim B_2$ [8], while any thermodynamic component should remain constant for a constant interfacial tension. Now the time spent at the interface is inversely proportional to Ca, while the hydrodynamic torque should scale linearly with Ca when β is constant, explaining the approximately equal exit angles observed in Fig. 5ii.

In the absence of perturbations, a single swimmer moves with a speed u_0 in a bulk fluid. To evaluate the effect of the presence of a liquid-liquid interface, we consider a velocity component $u_y(t) - u_0\sin\phi$ perpendicular to the interface (Fig. 6i). From the simulation data $u_y - u_0\sin\phi$ (Fig. 6i), a trapping energy can be estimated as, $\Delta E^p_{\mathrm{sim}} = -\mu_{\mathrm{trans}}\int(u_y - u_0\sin\phi_0)dy$ (Fig. 6ii). In an ideal situation, in the absence of hydrodynamic flows ($\mathrm{Ca} \approx 0$), one would expect a smooth parabolic potential with a minimum at the middle of the interface(i.e., $h = 0$).

For reasonably small capillary numbers, we observe an initial speed up of the vertical velocity, followed by a smooth reduction of the speed (Fig. 6i). The integrated trapping potential is parabolic (see *e.g.* $\mathrm{Ca} \approx 0.03$ in Fig. 6 ii). When the Ca is increased, both the interface-induced variations in the particle velocity become non-monotonic (see *e.g.*, $\mathrm{Ca} \approx 0.075$ and 0.12 in Fig. 6i). Also the position of the trapping potential minimum deviates (rightward shift) significantly from the ideal case (Fig. 6ii). However, the maximum trapping energy, given by the potential minimum, remains more or less constant across the Ca considered, which implies a constant thermodynamic trapping due to a constant value of the interfacial tension and alignment angle ϕ.

This observation is consistent with the theoretical thermodynamic trapping potential $\Delta E^p_{\mathrm{th}}(h,\phi)$ of a prolate swimmer (Eq. 8), which can be defined in terms of the A_{rm} as a function of the offset height h and alignment angle ϕ

$$\Delta E^p_{\mathrm{th}}(h,\phi) = -\sigma_0 A_{\mathrm{rm}}(h,\phi), \tag{8}$$

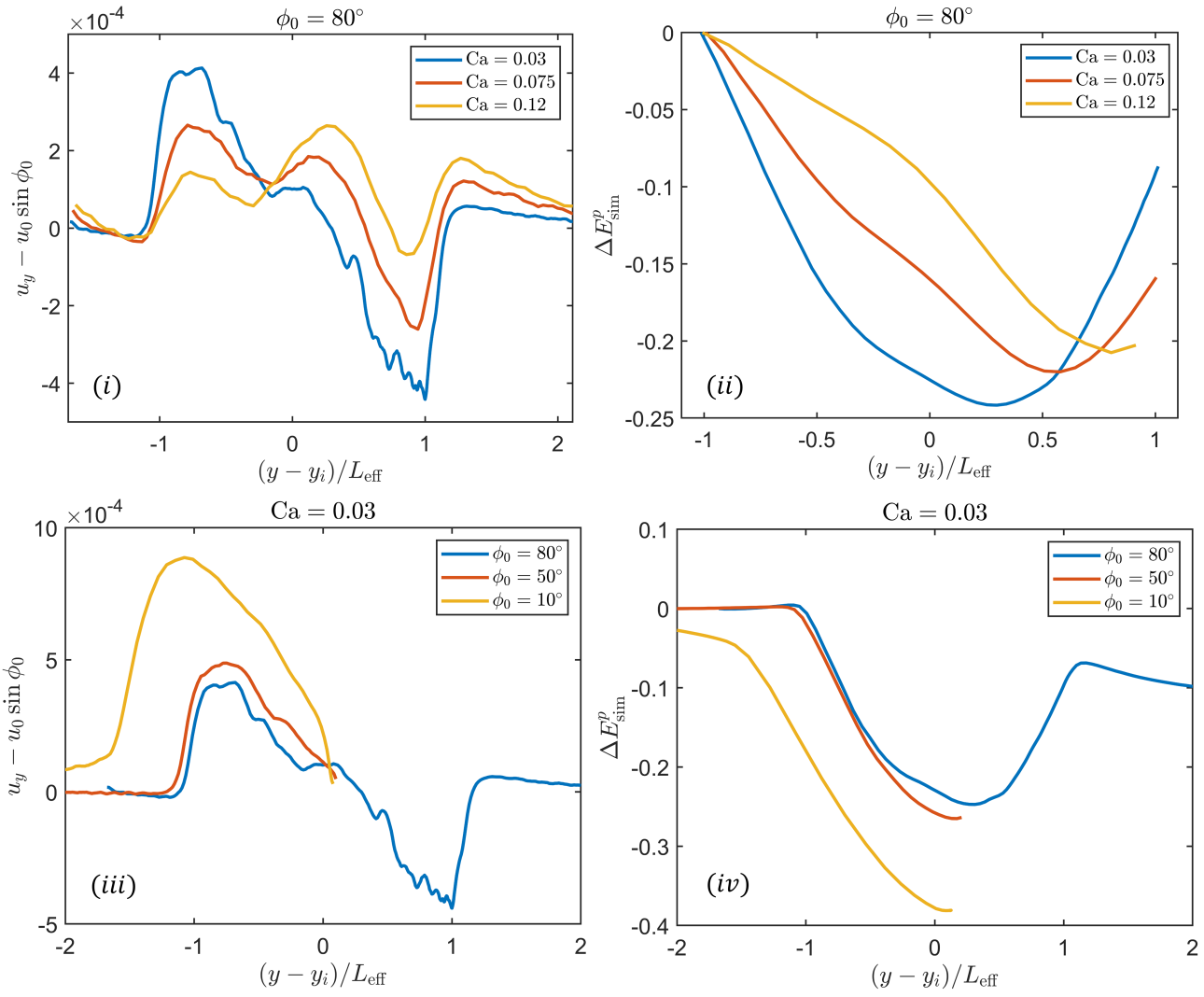

FIG. 6. (i) The velocity component perpendicular to the interface $u_y - u_0 \sin\phi_0$ for Ca $\approx$ 0.03, 0.075, 0.12 at fixed initial alignment $\phi_0 \approx 80°$. (ii) The corresponding calculated spatial trapping potential $\Delta E^p_{\text{sim}} = -\mu_{\text{trans}} \int (u_y - u_0 \sin\phi_0) dy$. (iii) and (iv) $u_y - u_0 \sin\phi_0$ and ΔE^p_{sim} for $\phi_0 \approx 10°,\ 50°,\ 80°$ at fixed Ca $\approx$ 0.03, respectively. The data corresponds to interfacial tension $\sigma_0 \approx 6\mu$N/m.

where,

$$A_{\text{rm}}(\phi, h) = \begin{cases} \frac{\pi a b^2 [(a^2 \sin^2\phi + b^2 \cos^2\phi) - h^2]}{(a^2 \sin^2\phi + b^2 \cos^2\phi)^{\frac{3}{2}}}, & \text{if } h^2 < a^2 \sin^2\phi + b^2 \cos^2\phi \\ 0, & \text{otherwise} \end{cases} \tag{9}$$

The cutoff corresponds to the half-length of the ellipsoid perpendicular to the interface $L_{\text{eff}} = \sqrt{a^2 \sin^2\phi + b^2 \cos^2\phi}$.

As the eq. 8 suggests, the potential energy depends on the alignment angle ϕ, where the maximum trapping is predicted for swimmers parallel to the interface $\phi \approx 0$. Our simulations agree with this. For a constant value of capillary number, Ca $\approx$ 0.03, reduction in ϕ_0 from angles close to interface normal *i.e.* 90° to a shallow angles 10°, a larger velocity component normal to the interface (Fig. 6iii) consequently a deeper potential is observed (Fig. 6iv).

We can also calculate the evolution of the binary fluid free energy (Eq. 2) as a function of the particle's distance, y, from the interface. Now the trapping potential ΔE^p can be extracted by calculating the difference in thermodynamic free energy when the swimmer is in the interface interaction region and the bulk region (Fig. 7). Using this method, we obtained reasonable quantitative agreement between the theoretical potential Eq. 8 (solid lines in Fig. 7). Comparing the simulations and theoretical results, it is observed that that in the simulations the effective

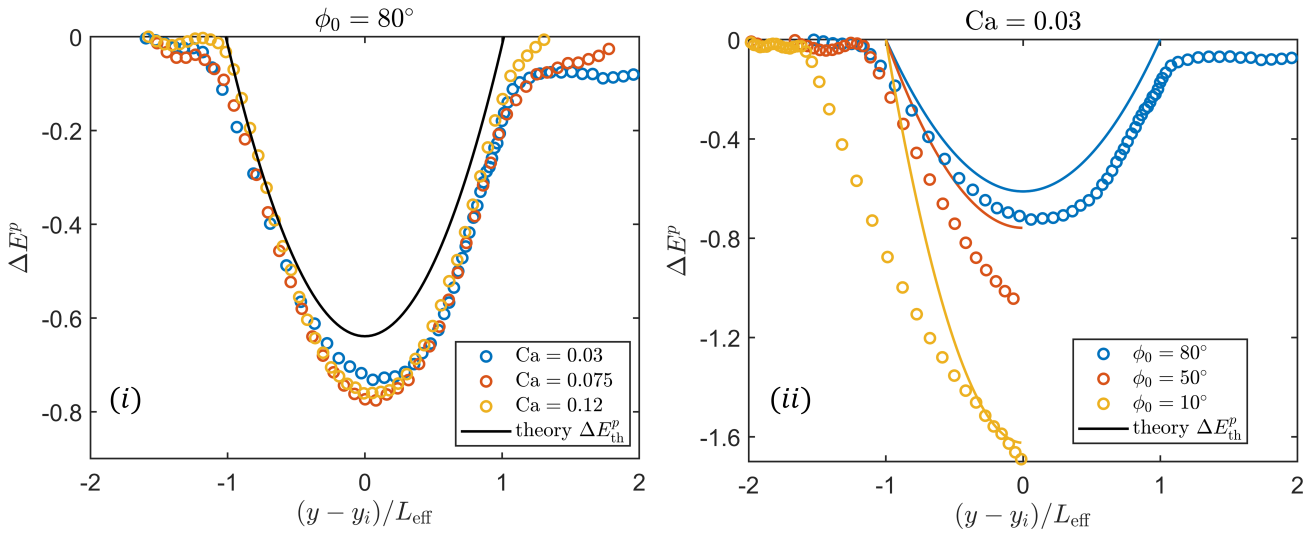

FIG. 7. The trapping potential ΔE^p calculated from the binary fluid free energy (Eq. 2; see text for details, where $\Delta E^p = F(\text{bulk}) - F(\text{particle at interface})$). (i) ΔE^p as a function of the particle position y for various capillary numbers Ca at fixed $\phi_0 = 80°$. (ii) ΔE^p for a range of ϕ_0 at fixed Ca ≈ 0.03. The simulations were carried out with a constant interfacial tension $\sigma_0 \approx 6$ μN/m.

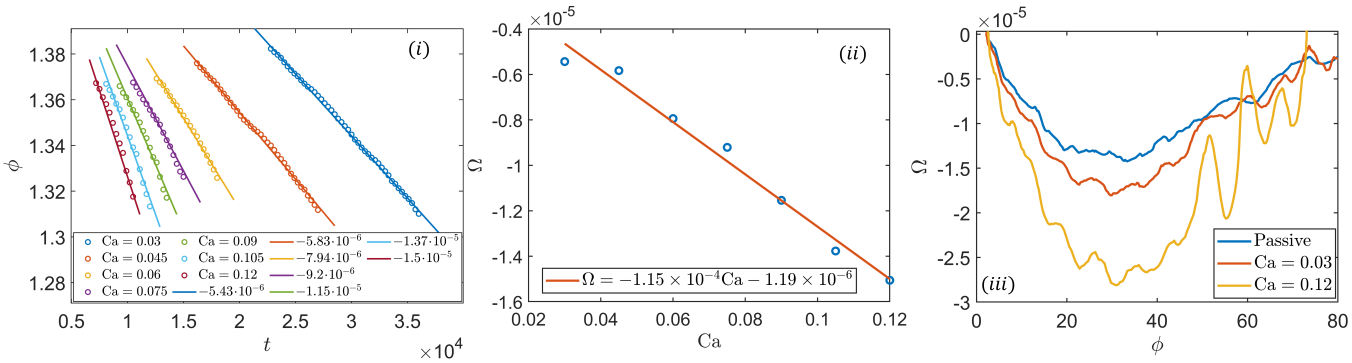

FIG. 8. Rate of reorientation of a prolate swimmer interacting with a fluid–fluid interface with an initial alignment angle $\phi_0 \approx 80°$. (i) The temporal evolution of the orientation angle ϕ (in radians), the solid lines represent the linear fit, from which the slope (Ω) has been obtained. (ii) The reorientation rate $\Omega = \dfrac{d\phi}{dt}$ calculated from the linear fits in (i) as a function of the capillary number (Ca). (iii) The reorientation rate Ω calculated for a passive ellipsoid (blue line) and two ellipsoidal shakers $B_1 = 0, B_2 \neq 0$ corresponding to Ca ≈ 0.03 and 0.12 (see text for details). The simulations correspond to aspect ratio $AR = a/b = 3$ and interfacial tension $\sigma_0 \approx 6$ μN/m.

range of swimmer–interface interaction is larger than $L_{\text{eff}}(\phi_0)$. This is especially visible for shallow angles, particularly at $\phi_0 = 10°$ (yellow symbols in Fig. 7ii). This discrepancy can be understood considering the phase trajectory (y vs ϕ) of the swimmer (Fig. 3iii). For the initial angle $\phi_0 \approx 10$, it is observed that below the interface swimmer is reorienting perpendicular to the interface, reaching a maximum alignment angle $\phi \approx 30$ and thus increasing its L_{eff}. A similar reorienting behavior towards the interface normal is also reported in the bacterial experiments [6]. This reorientation is likely due to a hydrodynamic torque, τ_{hydro}, arising from the coupling between the far-field flow-fields of the swimmer and the interface. The increased angle ϕ makes the apparent $L_{\text{eff}}(t) > L_{\text{eff}}(\phi_0)$, thus the particle surface reaches the interface at distances $y > L_{\text{eff}}(\phi_0)$.

The integrated potentials from the particle dynamics (Fig. 6) agree qualitatively with the potentials calculated from the free energy (Fig. 7). However, in the case of particle dynamics, the apparent maximum trapping energy is reduced. This is likely due to hydrodynamic interactions between the swimmer and the interface. It should also be noted that in the integration, a constant drag coefficient $\mu_{\text{trans}} = \frac{4\pi\eta a}{\ln \frac{2a}{b} - 0.5}$ corresponding to a prolate particle moving

along its long axis [40], was used. However, the drag coefficient itself likely depends on the distance and other details when the particle is near an interface [41–44]. Despite these discrepancies, all the data support the idea of trapping the swimmers via wetting-induced thermodynamic potential, akin to thermodynamic trapping of passive colloidal particles at interfaces [31].

Previous studies have proposed, that spherical pusher-type microswimmers at an interface with no viscosity contrast tend to align parallel to the interface due to a hydrodynamic torque arising from the force dipole B_2 flows [8, 9]. We assume a similar mechanism in our rod-like swimmers as well. However, the torque for a prolate-shaped particle should also include a thermodynamic component τ_{thermo}, aligning the long axis of the ellipsoid along the interface. To evaluate the reorientation of the swimmers, we considered swimmers crossing the interface with an initial alignment angle $\phi_0 \approx 80$ for various capillary numbers $\text{Ca} \approx 0.03 \ldots 0.12$ (Fig. 8), for a fixed interfacial tension σ_0. In all the cases, the swimmers were observed to reorient towards the interface (Fig. 8i), with the reorientation rate increasing linearly with the capillary number (Fig. 8ii). To study the reorientation in more detail, passive particle and two shakers ($B_1 = 0$; $B_2 \neq 0$) corresponding to $\text{Ca} = \eta B_2/\sigma_0 \approx 0.03$ and 0.12 were considered (Fig. 8iii). In all the cases, the particles were initialized in the middle of the interface with an initial alignment $\phi_0 \approx 80$. The results agree qualitatively with what is expected. The swimmer with the largest Ca, corresponding to highest force dipole strength B_2, is observed to rotate fastest, while the passive ellipsoid is the slowest. This suggests that the reorientation arises from a torque τ with both thermodynamic and hydrodynamic components $\tau = \tau_{\text{thermo}} + \tau_{\text{hydro}}$, where $\tau_{\text{hydro}} \sim B_2$ and $\tau_{\text{thermo}} \sim -\frac{\partial \Delta E^p}{\partial \phi_\cdot}$.

C. Conclusions

We have investigated the dynamics of a prolate-shaped microswimmer approaching a liquid-liquid interface between two Newtonian fluids. We observe that the swimmer can either be trapped or cross the interface, depending on its swimming speed, orientation angle, and the interfacial tension between the two fluids. We propose a model, where the swimmers are trapped due to a wetting induced thermodynamic trapping potential, similar to the thermodynamic trapping of passive colloidal particles at liquid-liquid interfaces [31]. Now, the trapping dynamics of the swimmer can be understood by balancing swimming (self-propulsion) and interfacial forces by considering a capillary number $\text{Ca} = u_0\eta/\sigma_0$, which gives the ratio between these. Further, our results demonstrate that the reorientation of the swimmers occurs via combined hydrodynamic and thermodynamic torques, which both rotate the swimmer parallel to the interface. The hydrodynamic torque that arises from the force dipole B_2 term increases linearly with Ca for $\beta \approx -1$ swimmers, whereas the thermodynamic torques remain constant for a fixed aspect ratio AR and interfacial tension. We anticipate that the result presented might be applicable to a wide variety of systems, including artificial or bacterial swimmers traversing clean liquid-liquid interfaces.

ACKNOWLEDGMENTS

The authors gratefully acknowledge the High Performance Computing (HPC) support provided by AGASTYA at IIT Jammu, India, and CURTA at MCIA, France, for facilitating the computational resources used in this work.

[1] J. Elgeti, R. G. Winkler, and G. Gompper, Physics of microswimmers—single particle motion and collective behavior: a review, Reports on Progress in Physics **78**, 056601 (2015).
[2] A. Purushothaman and S. P. Thampi, Hydrodynamic collision between a microswimmer and a passive particle in a microchannel, Soft matter **17**, 3380 (2021).
[3] V. A. Shaik and A. M. Ardekani, Motion of a model swimmer near a weakly deforming interface, Journal of Fluid Mechanics **824**, 42 (2017).
[4] S. Nambiar and J. S. Wettlaufer, Hydrodynamics of slender swimmers near deformable interfaces, Physical Review Fluids **7**, 054001 (2022).
[5] J. Deng, M. Molaei, N. G. Chisholm, and K. J. Stebe, Interfacial flow around a pusher bacterium, Journal of Fluid Mechanics **976**, A18 (2023).
[6] J. Cheon, J. Son, S. Lim, Y. Jeong, J.-H. Park, R. J. Mitchell, J. U. Kim, and J. Jeong, Motile bacteria crossing liquid–liquid interfaces of an aqueous isotropic–nematic coexistence phase, Soft Matter **20**, 7313 (2024).
[7] J. Cheon, K. H. Choi, K. J. Modica, R. J. Mitchell, S. C. Takatori, and J. Jeong, Motility modulates the partitioning of bacteria in aqueous two-phase systems, Phys. Rev. Lett. **135**, 128401 (2025).

[8] H. Gidituri, Z. Shen, A. Würger, and J. S. Lintuvuori, Reorientation dynamics of microswimmers at fluid-fluid interfaces, Physical Review Fluids **7**, L042001 (2022).

[9] C. Feng, J. J. Molina, M. S. Turner, and R. Yamamoto, Dynamics of microswimmers near a soft penetrable interface, Physical Review Research **4**, 043202 (2022).

[10] C. Feng, J. J. Molina, M. S. Turner, and R. Yamamoto, Dynamics of microswimmers near a liquid–liquid interface with viscosity difference, Physics of Fluids **35**, 051903 (2023).

[11] H. Gidituri, A. Würger, K. Stratford, and J. S. Lintuvuori, Dynamics of a spherical colloid at a liquid interface: A lattice boltzmann study, Physics of Fluids **33**, 052110 (2021).

[12] W. Fei, Y. Gu, and K. J. Bishop, Active colloidal particles at fluid-fluid interfaces, Current Opinion in Colloid and Interface Science **32**, 57 (2017).

[13] J. Deng, M. Molaei, N. G. Chisholm, and K. J. Stebe, Motile bacteria at oil–water interfaces: Pseudomonas aeruginosa, Langmuir **36**, 6888 (2020).

[14] J. Deng, M. Molaei, N. G. Chisholm, S. E. Clarke, and K. J. Stebe, Swimmers at interfaces enhance interfacial transport, Soft Matter **20**, 5245 (2024).

[15] L. Vaccari, M. Molaei, T. H. Niepa, D. Lee, R. L. Leheny, and K. J. Stebe, Films of bacteria at interfaces, Advances in Colloid and Interface Science **247**, 561 (2017).

[16] D. F. Williams and J. C. Berg, The aggregation of colloidal particles at the air—water interface, Journal of Colloid and Interface Science **152**, 218 (1992).

[17] P. Pieranski, Two-dimensional interfacial colloidal crystals, Phys. Rev. Lett. **45**, 569 (1980).

[18] K. Du, E. Glogowski, T. Emrick, T. P. Russell, and A. D. Dinsmore, Adsorption energy of nano- and microparticles at liquid-liquid interfaces, Langmuir **26**, 12518 (2010).

[19] N. Desai and A. M. Ardekani, Biofilms at interfaces: microbial distribution in floating films, Soft Matter **16**, 1731 (2020).

[20] J. Li, S. Thamphiwatana, W. Liu, B. Esteban-Fernaández de ´ Avila, P. Angsantikul, E. Sandraz, J. Wang, T. Xu, F. Soto, V. Ramez, *et al.*, Enteric micromotor can selectively position and spontaneously propel in the gastrointestinal tract, ACS nano **10**, 9536 (2016).

[21] W. Gao, X. Feng, A. Pei, Y. Gu, J. Li, and J. Wang, Seawater-driven magnesium based janus micromotors for environmental remediation, Nanoscale **5**, 4696 (2013).

[22] L. Soler, V. Magdanz, V. M. Fomin, S. Sanchez, and O. G. Schmidt, Self-propelled micromotors for cleaning polluted water, ACS Nano **7**, 9611 (2013).

[23] B. Jurado-Sánchez, S. Sattayasamitsathit, W. Gao, L. Santos, Y. Fedorak, V. V. Singh, J. Orozco, M. Galarnyk, and J. Wang, Self-propelled activated carbon janus micromotors for efficient water purification, Small **11**, 499 (2015).

[24] N. G. Chisholm and K. J. Stebe, Driven and active colloids at fluid interfaces, Journal of Fluid Mechanics **914**, A29 (2021).

[25] A. M. Menzel, A. Saha, C. Hoell, and H. Löwen, Dynamical density functional theory for microswimmers, The Journal of Chemical Physics **144**, 024115 (2016).

[26] K. Ishimoto and E. A. Gaffney, Squirmer dynamics near a boundary, Phys. Rev. E **88**, 062702 (2013).

[27] P. Malgaretti, M. Popescu, and S. Dietrich, Active colloids at fluid interfaces, Soft Matter **12**, 4007 (2016).

[28] R. Mishra, M. Gosika, H. Gidituri, and H. Pothukuchi, Flow structure around a microswimmer at fluid–fluid interface, Fluid Dynamics Research **56**, 045507 (2024).

[29] N. Desai, V. A. Shaik, and A. M. Ardekani, Hydrodynamics-mediated trapping of micro-swimmers near drops, Soft matter **14**, 264 (2018).

[30] S. Nambiar and J. S. Wettlaufer, Stochastic reorientations and the hydrodynamics of microswimmers near deformable interfaces, Phys. Rev. Fluids **9**, 023102 (2024).

[31] B. P. Binks and S. O. Lumsdon, Influence of particle wettability on the type and stability of surfactant-free emulsions, Langmuir **16**, 8622 (2000).

[32] J.-C. Desplat, I. Pagonabarraga, and P. Bladon, Ludwig: A parallel lattice-boltzmann code for complex fluids, Computer Physics Communications **134**, 273 (2001).

[33] V. M. Kendon, M. E. Cates, I. Pagonabarraga, J.-C. Desplat, and P. Bladon, Inertial effects in three-dimensional spinodal decomposition of a symmetric binary fluid mixture: a lattice boltzmann study, Journal of Fluid Mechanics **440**, 147–203 (2001).

[34] M. Theers, E. Westphal, G. Gompper, and R. G. Winkler, Modeling a spheroidal microswimmer and cooperative swimming in a narrow slit, Soft Matter **12**, 7372 (2016).

[35] S. R. Keller and T. Y. Wu, A porous prolate-spheroidal model for ciliated micro-organisms, Journal of Fluid Mechanics **80**, 259–278 (1977).

[36] S. P. Thampi, K. Stratford, and O. Henrich, Simulating dynamics of ellipsoidal particles using lattice boltzmann method, Phys. Rev. E **109**, 065302 (2024).

[37] kevinstratford, O. Henrich, jlintuvuori, dmarendu, qikaifzj, austin1997, shanCHEN123, ludwig cf, jurijsab, S. G. Leyva, and sumeshpt, ludwig-cf/ludwig: Ludwig 0.22.0 (2024).

[38] Ludwig: A parallel lattice-boltzmann code for complex fluids, https://github.com/ludwig-cf/ludwig/releases/tag/ludwig-0.21.0.

[39] G. B. Davies, T. Krüger, P. V. Coveney, J. Harting, and F. Bresme, Interface deformations affect the orientation transition of magnetic ellipsoidal particles adsorbed at fluid–fluid interfaces, Soft Matter **10**, 6742 (2014).

[40] H. C. Berg, *Random walks in biology* (Princeton University Press, 1993).

[41] G. Boniello, A. Stocco, M. Gross, M. In, C. Blanc, and M. Nobili, Translational viscous drags of an ellipsoid straddling an interface between two fluids, Phys. Rev. E **94**, 012602 (2016).

[42] J.-C. Loudet, M. Qiu, J. Hemauer, and J. J. Feng, Drag force on a particle straddling a fluid interface: Influence of interfacial deformations, The European Physical Journal E **43**, 13 (2020).
[43] K. Danov, R. Aust, F. Durst, and U. Lange, Influence of the surface viscosity on the drag and torque coefficients of a solid particle in a thin liquid layer, Chemical Engineering Science **50**, 263 (1995).
[44] K. Danov, T. Gurkov, H. Raszillier, and F. Durst, Stokes flow caused by the motion of a rigid sphere close to a viscous interface, Chemical Engineering Science **53**, 3413 (1998).